Ocean Dynamics (2014) 64:1193–1207
DOI 10.1007/s10236-014-0719-4

# Observations and modeling of surf zone transverse finger bars at the Gold Coast, Australia

**F. Ribas · A. ten Doeschate · H. E. de Swart · B. G. Ruessink · D. Calvete**

Received: 1 December 2013 / Accepted: 7 April 2014 / Published online: 23 July 2014


**Abstract** The occurrence and characteristics of transverse finger bars at Surfers Paradise (Gold Coast, Australia) have been quantified with 4 years of time-exposure video images. These bars are attached to the inner terrace and have an oblique orientation with respect to the coastline. They are observed during 24 % of the study period, in patches up to 15 bars, with an average lifetime of 5 days and a mean wavelength of 32 m. The bars are observed during obliquely incident waves of intermediate heights. Bar crests typically point toward the incoming wave direction, i.e., they are up-current oriented. The most frequent beach state when bars are present (43 % of the time) is a rhythmic low-tide terrace and an undulating outer bar. A morphodynamic model, which describes the feedback between waves, currents, and bed evolution, has been applied to study the mechanisms for finger bar formation. Realistic positive feedback leading to the formation of the observed bars only occurs if the sediment resuspension due to roller-induced turbulence is included. This causes the depth-averaged sediment concentration to decrease in the seaward direction, enhancing the convergence of sediment transport in the offshore-directed flow perturbations that occur over the up-current bars. The longshore current strength also plays an important role; the offshore root-mean-square wave height and angle must be larger than some critical values (0.5 m and 20°, respectively, at 18-m depth). Model-data comparison indicates that the modeled bar shape characteristics (up-current orientation) and the wave conditions leading to the bar formation agree with data, while the modeled wavelengths and migration rates are larger than the observed ones. The discrepancies might be because in the model we neglect the influence of the large-scale beach configuration.

**Keywords** Surf zone morphodynamics · Transverse finger bars · Video remote sensing · Linear stability analysis · Gold Coast

Responsible Editor: Bruno Castelle

This article is part of the Topical Collection on the *7th International Conference on Coastal Dynamics in Arcachon, France 24-28 June 2013*

F. Ribas (✉) · D. Calvete
Applied Physics Department, Universitat Politècnica de Catalunya, Barcelona, Spain
e-mail: francesca.ribas@upc.edu

D. Calvete
e-mail: daniel.calvete@upc.edu

A. ten Doeschate · H. E. de Swart
Institute for Marine and Atmospheric Research Utrecht, Utrecht University, Utrecht, Netherlands
e-mail: h.e.deswart@uu.nl

B. G. Ruessink
Faculty of Geosciences, Department of Physical Geography, Utrecht University, Utrecht, Netherlands
e-mail: B.G.Ruessink@uu.nl

*Present Address:*
A. ten Doeschate
School of Physics, National University of Ireland Galway, Dublin, Ireland

## 1 Introduction

Sandy beaches often display pronounced morphological features, such as crescentic sandbars and rip channels. In this contribution, the focus is on the less well-known transverse finger bars: relatively small, shore-oblique bars that are attached to an inner sandbar or to the shoreline. Observations from Duck, USA (Konicki and Holman 2000)

and Noordwijk, the Netherlands (Ribas and Kroon 2007) indicate finger bars to be relatively rare features (they were present 10–15 % of the time) with a typical alongshore wavelength ranging from 20 to 200 m. Finger bars migrate at rates up to 2 m/h in the direction of the longshore current. Ribas and Kroon (2007) also correlated the wavelength, crest orientation, and migration rate of Noordwijk bars with quantities derived from hourly wave conditions measured at an 18-m depth buoy. Crests of finger bars were obliquely oriented from the shore-normal in the upflow direction ("up-current orientation"). Offshore wave conditions detected in Noordwijk during bar presence were characterized as intermediate wave (root-mean-square (RMS) height, $H_{\mathrm{off}} = 0.75$ m) with large angles of incidence with respect to the shore-normal ($\theta_{\mathrm{off}} = 50°$). One to three shore-parallel subtidal bars are very often present in Duck and Noordwijk, sometimes showing a crescentic shape with undulations at length scales of hundreds of meters (van Enckevort et al. 2004).

Finger bars can form as a result of morphodynamic self-organization in the nearshore, i.e., due to the feedbacks between hydrodynamics (waves and currents) and bed evolution (Ribas et al. 2011a, b, 2012). These studies showed that accounting for the longshore currents generated by obliquely incident waves and wave rollers (which not only affect the currents but also generate additional sediment resuspension) is essential to successfully explain the formation of finger bars at Noordwijk (Ribas et al. 2011b, 2012) and at Duck (Ribas et al. 2011a). A depth-averaged sediment concentration that decreases in the seaward direction together with an offshore deflection of the longshore current over the up-current oriented bars are necessary conditions for the formation of finger bars. Ribas et al. (2011b) showed that including the roller-induced sediment resuspension creates an increase of the depth-averaged sediment concentration near the shoreline in such a way that this quantity decreases in the seaward direction across the inner surf zone.

Finger bars are the visible print of physical mechanisms that dominate the evolution of the morphology of the inner surf zone, a highly complex region. Studying their formation improves our understanding of the governing mechanisms in this region. These bars have up to now been studied at two beaches only, and the generality of the findings is unknown. In order to increase understanding of these features, it is essential to study their occurrence and characteristics in more beaches.

In this contribution, we extend knowledge of transverse finger bars by first examining a 4-year long data set of video images of Surfers Paradise beach (Gold Coast, Australia), where the persistent oblique incidence of the waves should be particularly beneficial to the formation of finger bars (Section 2). The aim is to quantify under what circumstances finger bars are formed there and to investigate their characteristics. The large-scale morphodynamic configuration of Surfers Paradise beach is very dynamic and can be described following the general classification of beach states (Wright and Short 1984), which was adapted to that beach by Price and Ruessink (2011). The latter study also showed that the inner bar/terrace and the outer bar are typically in a rhythmic coupled state, which is not the case at Duck and Noordwijk. The results of the data analysis are described in Section 3. In order to study the physical mechanisms behind finger bar formation, a morphodynamic model is subsequently used. The model, presented in Section 4, is applied to the bathymetric and offshore wave conditions measured at the Gold Coast during the periods when finger bars are observed. Model results, consisting of the initial shape, growth, and migration of different possible patterns, together with the beach conditions leading to bar formation, are described in Section 5. In Section 6, the modeling results are contrasted with the data, and we also include a comparison with the results obtained at Duck and Noordwijk. The contribution ends up with the conclusions (Section 7).

## 2 Study site and data set

The study site is at Surfers Paradise beach, Gold Coast, East Australia (Fig. 1). Surfers Paradise is a 20-km-long, more or less continuous stretch of beach, extending from Burleigh Heads in the south to the outfall of the Nerang

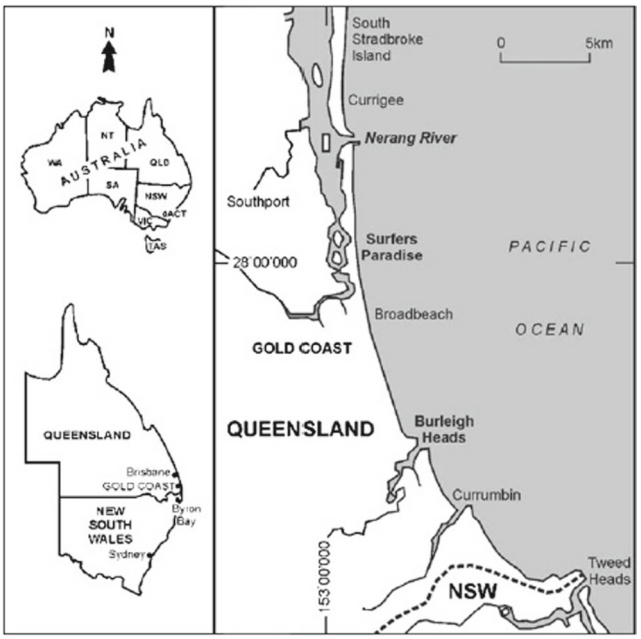


**Fig. 1** Location of Surfers Paradise beach, at the Gold Coast, East Australia

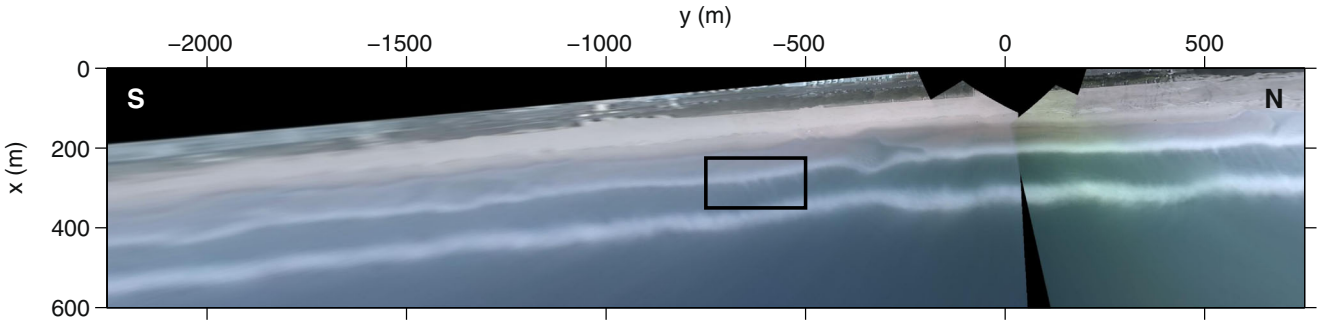


**Fig. 2** Argus time-exposure planview image on 07 June 2002, at 3 h GMT. The two alongshore parallel white lines are the zones of predominant wave breaking over the (bottom) outer shore-parallel bar and (top) inner terrace edge. Transverse finger bars can be seen attached to the terrace edge as the three small, obliquely oriented white stripes inside the black rectangle. The averaged wavelength of this patch is 32 m and bar crests point toward northeast. Waves were coming from the lower right corner

River in the north. The study site is located at the northern end of this beach and extends over 3 km. The coastline is aligned approximately north-south, and the beach is composed of predominantly quartz sand with a median grain size of 250 $\mu$m.

An Argus video system, consisting of four cameras spanning an 180° view of the coastline, was installed on top of a 100 m-high building (Ruessink et al. 2009). The Argus data used in the present study comprises 4-year series of daily, low-tide time-exposure video images. The planview images are obtained from the oblique camera images using standard photogrammetric techniques with a grid size of 1 m × 1 m (e.g., Fig. 2). The location of the camera system is used as the origin of the coordinate system. The specific time period studied, from 1 November 1999 to 31 October 2003, covers four winters and summers and corresponds to years during which some bathymetric data were collected. The data set of Argus images from the study period forms a nearly continuous series of images; for 1,430 days in total, there are only 59 days without any images of the beach.

Two bathymetric surveys of Surfers Paradise were performed during the study period, on 28 February 2001 and on 12 June 2002. The bathymetric measurements extend from the backside of the beach to about 800 m offshore. Figure 3 shows the 2002 bathymetry. We did not use the 2001 bathymetry in this study because no finger bars occurred close in time to the survey. As can be seen, the nearshore zone of the Gold Coast was characterized by an outer bar located at around 200 m from the mean shoreline and an inner terrace with the edge located at approximately 100 m from the shoreline. A more extensive account of sandbar dynamics at the Gold Coast is given in Ruessink et al. (2009).

The Gold Coast is relatively open, exposed to waves year-round. The long-term average offshore RMS wave height is 0.81 m, with higher than average waves between January and May, corresponding to the Australian summer and the cyclone season. The annual wave climate is dominated by swell generated in the Southern Ocean and Tasman Sea that impacts the coast as small to medium size, moderate to long period oblique waves, from the south to the southeast (Splinter et al. 2011). Hourly values of RMS wave height and period measured at the closest buoy, the Gold Coast buoy (located ay 18-m depth), were used. Since this buoy

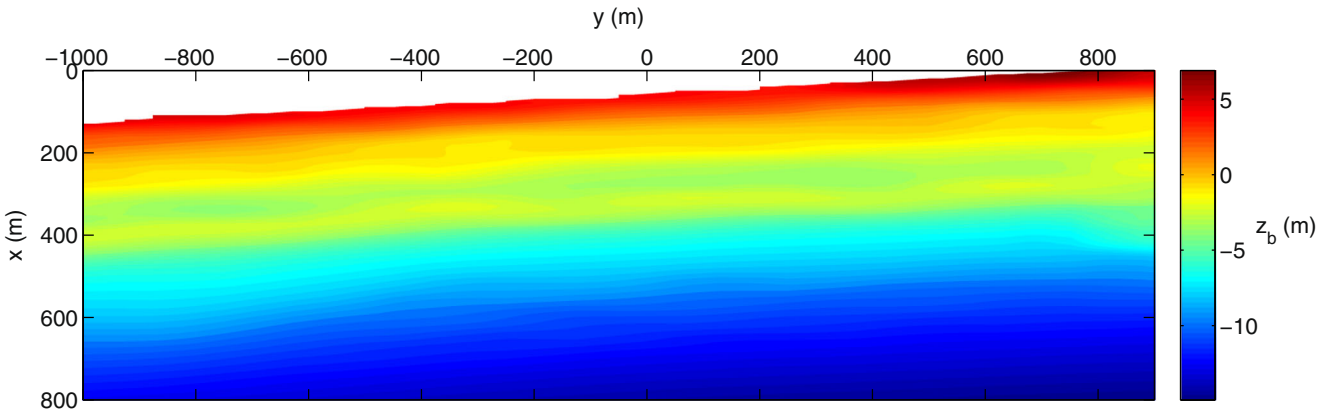


**Fig. 3** Bathymetric survey of Surfers Paradise on 12 June 2002, where the coordinate system is the same as in the Argus planview images (e.g., Fig. 2)

is not directional, data of wave direction were taken from the Brisbane offshore buoy (located at 80-m depth), and they were transformed to values at 18-m depth using Snell's law. The angle of wave incidence is defined with respect to the shore-normal and positive (negative) values which indicate that waves come from the south (north). Apart from providing directional information, the Brisbane wave recordings were used to fill up eventual measurement gaps in the Gold Coast buoy data. The wave conditions measured during the study period are shown in the two lower panels of Fig. 4.

## 3 Data analysis and results

### 3.1 Methods for data analysis

For every day of the study period, the time-exposure plan-view images around daily low tide were analyzed visually, tracking the occurrence of transverse finger bar events, their duration, the number of bars per event, the typical wavelength of the bars in a patch, and the crest orientation. A bar event was defined as that in which a bar patch with at least 3 bars could be continuously detected in a similar position over at least 2 days. This criterion for bar detection was chosen as the aim was to study alongshore rhythmic patches that were not too ephemeral. In order to quantify some of the bar characteristics, e.g., for estimating the wavelength with a sufficient reliability, a more restrictive criterion was imposed by defining "well developed" events. These were defined as those in which a patch of 3 or more bars was visible for more than 2 days, or a patch of more than 3 bars was visible for 2 days (e.g., Fig. 2). The wavelength of finger bars in each patch was measured—only for the well-developed events—as the alongshore averaged distance between bar crests (detected as maximum intensity locations due to preferable wave breaking over the finger bars). The wave conditions prior to the formation of finger bars were analyzed—only for well-developed events-by averaging wave height, period, and angle 24 h before the moment when finger bars became visible in the images for the first time in each event.

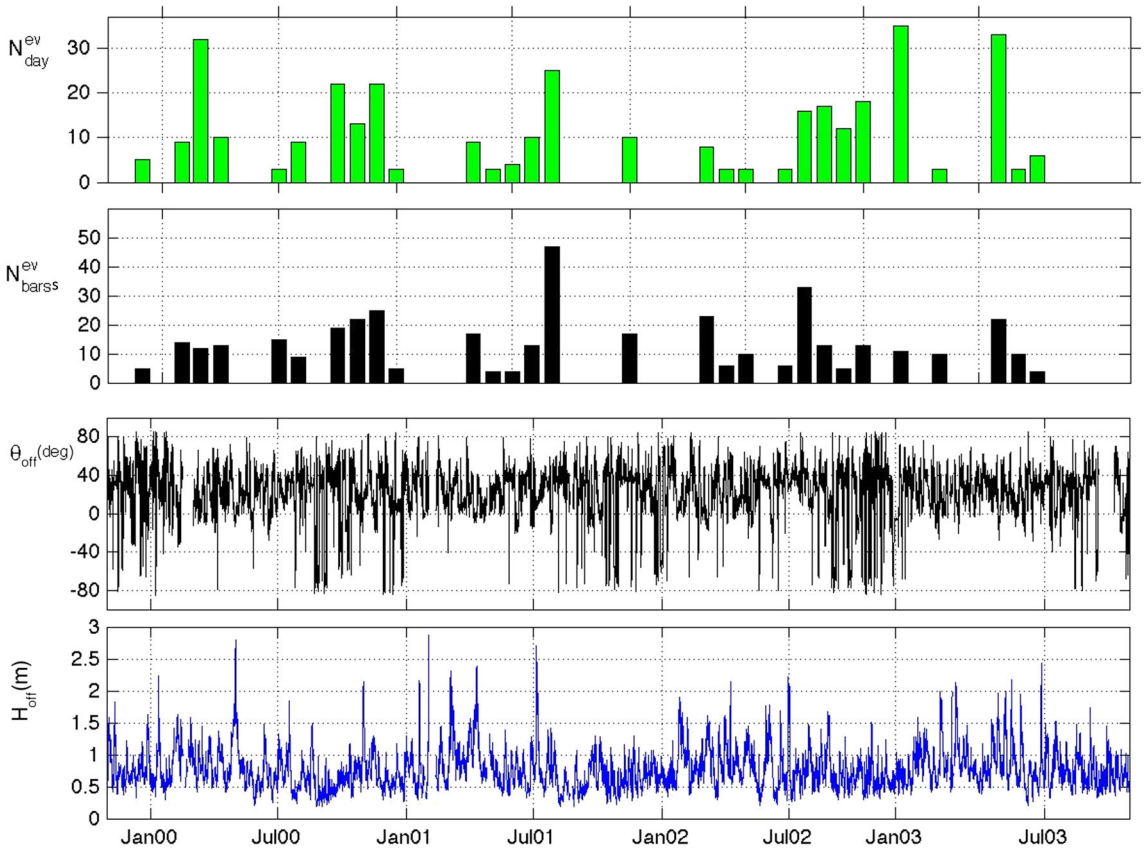


**Fig. 4** Monthly statistics of finger bar presence and wave conditions at 18-m depth during the study period. The *panels* show, from *top to bottom*, the monthly number of days with finger bar presence, $N^{ev}_{day}$, the total number of bars per month, $N^{ev}_{bars}$, the offshore angle of wave incidence with respect to shore-normal, $\theta_{off}$ (positive are waves from the south) and the offshore RMS wave height, $H_{off}$

### 3.2 Finger bar occurrence and characteristics

During the study period, 69 events of finger bar patches were observed, of which 35 were well-developed. In total, finger bars (that were part of an event) were observed during 24 % of the time (349 days). There was not a seasonal signal in the manifestation of finger bars (Fig. 4). During the Australian winter, there were slightly more events than during the summer but the difference is insignificant. Typically, patches comprised up to 15 bars (the average was 6 bars) attached to the low-tide terrace, with an average event duration of 5 days. An event with a maximum duration of 21 days was observed in March-April 2003.

The alongshore wavelength varied from 17 to 70 m, with a data set average value of 32 m. In most of the events (71 %), finger bars were oriented toward southeast (e.g., Fig. 5) and, in 27 % of the bar patches, they pointed toward northeast (e.g., Fig. 2). In the remaining cases, the orientation was more or less shore-normal or it could not be determined. From visual analysis, finger bar patches at Surfers Paradise did not seem to migrate significantly along the coast and quantitative migration rates were not evaluated.

### 3.3 Beach conditions during finger bar presence

As shown in Table 1, the ranges of offshore wave conditions during the study period were RMS heights ($H_{\text{off}}$) varying from 0.2 to 2.86 m, peak periods ($T_{\text{p}}$) from 3 to 22.5 s, and absolute values of the wave angle ($\theta_{\text{off}}$) from 0 to 85°. There was a clear dominance of southern waves, observed 85 % of the time (Fig. 6). The wave conditions prior to the formation of finger bars were also analyzed. The $H_{\text{off}}$ prior to the events never exceeded 1.2 m, with an average of 0.7 m, and the $T_{\text{p}}$ varied from 5.5 to 13 s, with an average of 9 s, indicating finger bars to be low to intermediate wave-energy features. The dominant angle of incidence measured with respect to the shore-normal prior to bar formation had an average value of 28° and a standard deviation of 16°, with a dominance of waves from southern directions. Orientation of bar crests was also quantitatively compared with the angle of wave incidence prior to the formation, showing that finger bars were typically up-current oriented. In 86 % of the events where bars pointed toward the southeast, waves were coming from southeastern directions. In 79 % of the events where bars were oriented toward the northeast, waves were coming from northeastern directions.

**Table 1** Offshore wave conditions at Surfers Paradise during the whole study period and prior to finger bar observation

| Wave conditions during the study period | | | |
|---|---|---|---|
| Quantity | Range | Mean | $\sigma$ |
| $H_{\text{off}}$ (m) | 0.18–2.86 | 0.77 | 0.32 |
| $T_{\text{p}}$ (s) | 2.88–22.5 | 9.37 | 2.48 |
| $\theta_{\text{off}}$ (deg) | 0.0–85.0 | 30.0 | 18.4 |
| Wave conditions prior to finger bar observation | | | |
| Quantity | Range | Mean | $\sigma$ |
| $H_{\text{off}}$ (m) | 0.31–1.23 | 0.71 | 0.20 |
| $T_{\text{p}}$ (s) | 5.50–13.1 | 9.27 | 1.78 |
| $\theta_{\text{off}}$ (deg) | 1.0–62.6 | 27.5 | 16.0 |

Finally, the relationship between the presence of finger bars and the large-scale bathymetric configuration of Surfers Paradise beach was studied. A preexisting data set was used where the states of the inner bar/terrace and the outer bar were quantified (Price and Ruessink 2011). The frequency of occurrence of bar state combinations of the inner terrace and the outer bar during the whole study period (1999–2003) can be seen in dark blue color in Fig. 7. The short and long names of the different bar states and the coding used in the horizontal axis of the latter figure to describe the combined states of the terrace and the outer bar is specified in Table 2. A detailed study of bar states at the Gold Coast is given in Price and Ruessink (2011). The large-scale alongshore variability occur at the length scales

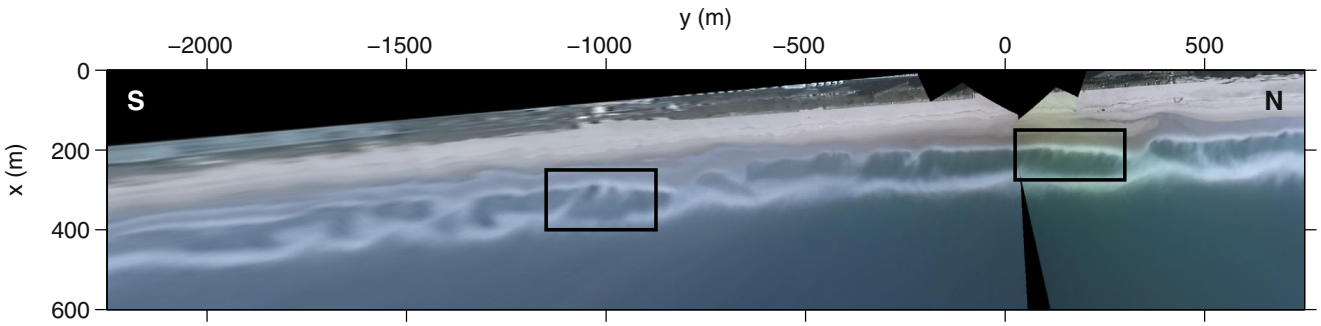


**Fig. 5** Argus time-exposure planview image on 27 May 2002, at 3 h GMT. Two finger bar events, which can be seen inside the *two black rectangles*, occurred while the terrace was in a rLLT state and the outer bar in a TBR state, the most frequent situation (bar state combination d5 in Fig. 7)

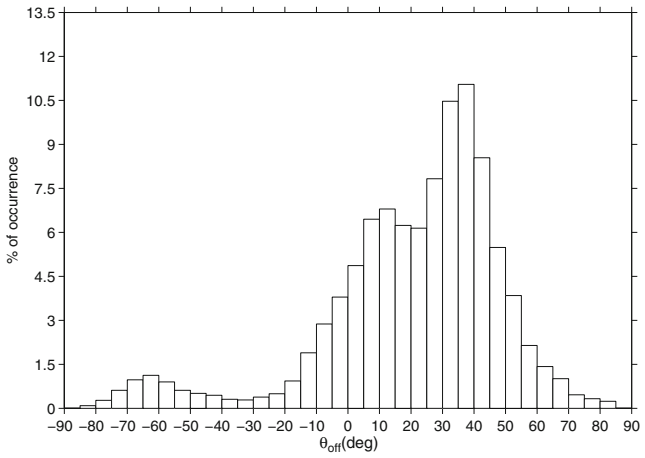


**Fig. 6** Frequency (in %) of occurrence of offshore wave angle during the study period, as recorded by the Brisbane directional wave buoy (80-m depth). Here, $\theta = 0°$ are shore-normal waves and $\theta > 0°$ are waves coming from southern directions

of a few hundreds of meters both in the terrace and the outer bar (Ruessink et al. 2007). The relationship between finger bar presence and large-scale beach configuration is also shown in Fig. 7, where the frequency of occurrence of bar state combinations at the start of well-developed finger bar events can be seen in light blue color. The combined beach states occurring most frequently when finger bars were present were formed by a rhythmic terrace—rLTT state—and a strongly undulating outer bar, either in a TBR state (32 % of the time, code d5 in Fig. 7) or in a RBB state (11 % of the time, code d4). In particular, Fig. 7 indicates that the large-scale beach configuration described as the state d5 might favor finger bar formation. An example of this situation is shown in Fig. 5. Notice that both finger bars and the combined beach states d4 and d5 are typical of low to intermediate wave conditions. As can be also seen in Fig. 5, finger bars were nearly always observed in the shoreward pointing embayments of the rhythmic terrace edge and rarely at its seaward directed perturbations.

## 4 Model formulation

The results obtained from the data analysis lead to an important question: is the initial formation of finger bars at the Gold Coast due to self-organization mechanisms? And, more specifically, can Gold Coast bars be explained by the same self-organization mechanisms that successfully explained finger bar formation at Duck and Noordwijk? This question is especially relevant in this site because the potential coupling of finger bars and the large-scale beach configuration can also be a factor controlling finger bar formation. As a first step, employing the self-organization model of Ribas et al. (2012) (Morfo62), that successfully explained finger bar formation at Duck and Noordwijk, can provide some answers. Also, this model, based on linear stability analysis, allows for checking the sensitivity of the results to varying the parameters in a wide range. And it can give insight on why finger bars at the Gold Coast form during obliquely incident waves of intermediate heights.

The model Morfo62 describes the feedback between wave and roller dynamics, depth-averaged currents, and bed evolution. The $y$ (or $x_2$) axis is chosen to coincide with the rectilinear shoreline and points toward the north (considering it represents Surfers Paradise beach), the $x$ (or $x_1$) axis points in the seaward direction and the $z$ axis points upwards. A summary of the model equations are described below and more details are given in Ribas et al. (2012).

### 4.1 Hydrodynamic equations

The depth-averaged currents are governed by the depth-averaged mass and momentum balance equations

$$\frac{\partial D}{\partial t} + \frac{\partial}{\partial x_j}\left(D v_j\right) = 0\,, \quad j = 1, 2\,, \tag{1}$$

$$\frac{\partial v_i}{\partial t} + v_j \frac{\partial v_i}{\partial x_j} = -g\frac{\partial z_s}{\partial x_i} - \frac{1}{\rho D}\frac{\partial}{\partial x_j}\left(S_{ij}^w + S_{ij}^r - S_{ij}^t\right) - \\ -\frac{\tau_{bi}}{\rho D} + \frac{\tau_{wi}}{\rho D}\,, \quad i, j = 1, 2\,. \tag{2}$$

Here, $v_j$ are the components of the depth-averaged water velocity $\vec{\mathbf{v}}$, and $D = z_\mathrm{s} - z_\mathrm{b}$ is the water depth, where $z_\mathrm{s}$ is the mean free surface elevation and $z_\mathrm{b}$ is the sea bottom level. In the equations, Einstein summation convention is used. Furthermore, $\tau_{bi}$ are the bed shear stresses, $S_{ij}^w$ and $S_{ij}^r$

**Table 2** Short and long names of the bar states and coding used in Fig. 7

| Short name | Long name | Code inner | Code outer |
|---|---|---|---|
| D | Dissipative | – | 1 |
| LBT | Longshore bar and trough | a | 2 |
| eTBR | Erosive transverse bar and rip | – | 3 |
| RBB | Rhythmic bar and beach | b | 4 |
| TBR | Transverse bar and rip | c | 5 |
| rLTT | Rhythmic low tide terrace | d | – |
| LTT | Low tide terrace | e | – |
| R | Reflective | f | – |

The "code inner" is used to indicate the state of the inner terrace/bar and the "code outer" is used to indicate the state of the outer bar. When the bar is never in a state, the symbol - is written

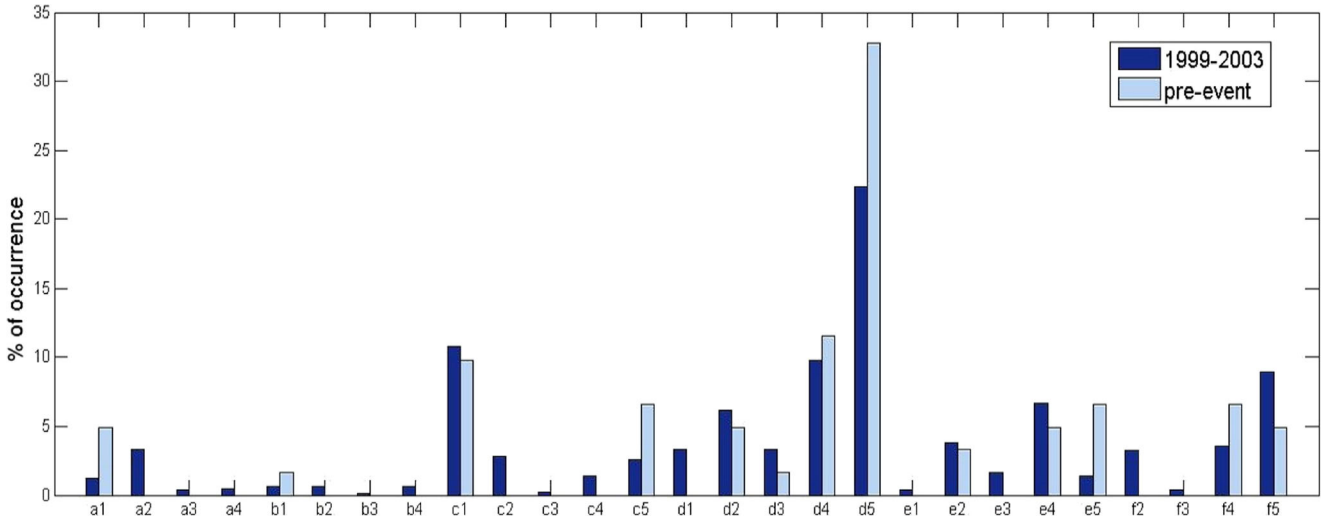


**Fig. 7** Frequency (in %) of occurrence of bar state combinations of the inner terrace and the outer bar during the whole study period (*dark blue*) and only at the start of the finger bar events (*light blue*). The coding used in the horizontal axis is shown in Table 2

are wave and roller radiation stresses, and $S^t_{ij}$ are the turbulent Reynolds stresses. All the equations and quantities are wave-averaged. The bed shear stresses are parameterized following the generalized equation developed by Feddersen et al. (2000), which has been extended to model the effect of a two-dimensional flow. The corresponding drag coefficient is assumed to vary with depth following the Manning-Strickler law (Soulsby 1997), where the apparent bed roughness, $k_a$, is constant and we use a range of realistic values (Table 3). The turbulent Reynolds stresses, $S^t_{ij}$ in Eq. (2), are modeled with the standard eddy viscosity approach. The lateral turbulent mixing coefficient $\nu_t$ is directly linked to the roller energy dissipation (the main source of turbulence in the area of interest), $\nu_t = M(\mathcal{D}^r/\rho)^{1/3}$, where $M$ is a parameter of order 1.

Waves are assumed to have a narrow spectrum in frequency and angle. Their heights are supposed to be random and follow the Rayleigh distribution, characterized by the RMS wave height, $H$ (wave energy density being $E = \rho g H^2/8$). When waves approach the coast, their evolution is described using linear wave theory, which yields expressions for the wave properties such as the wave radiation stresses, $S^w_{ij}$, the RMS wave orbital velocity amplitude near the bed, $u_b$, and the components of the phase speed, $c_i$, and the group velocity, $c_{gi}$. The intrinsic wave frequency is computed from the dispersion relation. When introducing the Doppler shift to relate the intrinsic frequency to the absolute frequency, $\omega_a$, the following relation is obtained,

$$\omega_a = \sqrt{g|\mathbf{K}|\tanh(|\mathbf{K}|D)} + v_j K_j \,, \quad j = 1, 2 \,. \tag{3}$$

Here, $K_j$ are the two components of the wave vector $\mathbf{K}$. Steady conditions are assumed, $\omega_a = \text{constant}$. Applying wavenumber irrotationality, Eq. (3) can be rewritten in terms of the wave phase $\Phi$, from which the two components of the wave vector can be computed, $K_i = \partial\Phi/\partial x_i$. The wave incidence angle with respect to shore-normal, $\theta$, is computed from the components of the wave vector. These wave propagation equations describe the refraction of the waves due to both topography and currents, but more complex processes, like wave diffraction, are not accounted for.

The wave energy balance reads

$$\frac{\partial E}{\partial t} + \frac{\partial}{\partial x_j}\big((v_j + c_{gj})E\big) + \\ + S^w_{jk}\frac{\partial v_k}{\partial x_j} = -\mathcal{D}^w \,, \quad j, k = 1, 2 \,. \tag{4}$$

An adequate parameterization of the energy dissipation rate due to wave breaking, $\mathcal{D}^w$, is critical. Here, the standard formulation by Thornton and Guza (1983) is used. The most important parameter is the saturation ratio of $H/D$, $\gamma_b$, which is assumed to be cross-shore uniform, and we use a range of realistic values (Table 3).

**Table 3** Default parameter setting and range of variation

| | Meaning | Default | Range |
|---|---|---|---|
| $\gamma_b$ | Saturation ratio of $H/D$ | 0.475 | 0.3–0.6 |
| $\beta_{rol}$ | Wave/roller front slope | 0.05 | 0.04–0.1 |
| $k_a$(m) | Apparent bed roughness | 0.035 | 0.01–0.1 |
| $M$ | Turbulence parameter | 1 | 0.1–10 |
| $n_{rol}$ | Roller stirring parameter | 40 | 0–90 |
| $H_{off}$(m) | Offshore wave height | 0.8 | 0.2–2 |
| $T_p$ (s) | Peak wave period | 9 | 3–16.5 |
| $\theta_{off}$(deg) | Offshore wave angle | 30° | 0–80° |

The energy dissipated by wave breaking feeds the surface rollers, i.e., the aerated mass of water located on the shoreward face of breaking waves. The depth-averaged roller energy balance is an extension of the one proposed by Reniers et al. (2004), which we have adapted to account for wave-current interactions,

$$\frac{\partial (2E^{\mathrm{r}})}{\partial t} + \frac{\partial}{\partial x_j}\left(2(v_j + c_j)E^{\mathrm{r}}\right) + \\ + S^r_{jk}\frac{\partial v_k}{\partial x_j} = -\mathcal{D}^{\mathrm{r}} + \mathcal{D}^w \,, \quad j,k = 1,2\,. \tag{5}$$

In this equation, $E^{\mathrm{r}}$ is the energy density of the rollers, $c_j$ are the components of the phase speed along the $x_j$ axis and $S^r_{ij}$ are the radiation stresses due to roller propagation, which are computed following (Svendsen 1984). Finally, the roller energy dissipation rate, $D^{\mathrm{r}}$, in Eq. (5) is modelled following (Ruessink et al. 2001), where the angle of the wave/roller interface, $\beta_{\mathrm{rol}}$, is assumed to be 0.1 or less.

### 4.2 Bed evolution and sediment transport

Conservation of sediment mass yields the bottom evolution equation

$$\frac{\partial z_{\mathrm{b}}}{\partial t} + \frac{1}{1-p}\frac{\partial q_j}{\partial x_j} = 0\,, \quad j = 1,2\,, \tag{6}$$

with $p = 0.4$ being the porosity of the bed and $q_i$ the two components of the depth-averaged volumetric sediment transport ($\mathrm{m}^2$/s). A widely accepted formulation for $q_i$ in the nearshore is that of Soulsby and van Rijn (Soulsby 1997). Their original expression has been extended to model the effect of a two-dimensional flow and to modify the preferred downslope transport of the sand,

$$q_i = \mathcal{C}\left(v_i - \Gamma\frac{\partial \hat{h}}{\partial x_i}\right)\,, \quad i = 1,2\,. \tag{7}$$

In this expression, $\mathcal{C}$ can be interpreted as the depth-integrated volumetric sediment concentration due to the stirring by waves and currents. The second term inside the parenthesis of Eq. (7), where $\Gamma$ is called bedslope coefficient, accounts for the tendency of the system to smooth out the sea bed perturbations, $\hat{h}$, if the latter do not cause positive feedback into the flow.

The depth-integrated concentration $\mathcal{C}$ in Eq. (7) reads

$$\mathcal{C} = A_{\mathrm{s}}\,(u_{\mathrm{stir}} - u_{\mathrm{crit}})^{2.4}\,, \quad \text{if} \quad u_{\mathrm{stir}} > u_{\mathrm{crit}}\,, \\ \mathcal{C} = 0 \qquad\qquad\qquad\quad , \quad \text{otherwise}\,. \tag{8}$$

Here, the parameter $A_{\mathrm{s}}$ accounts for the sediment properties, $u_{\mathrm{crit}}$ is the threshold flow intensity for sediment transport, and $u_{\mathrm{stir}}$ is a representative stirring velocity responsible for sediment resuspension. The full expressions for $u_{\mathrm{crit}}$ and $A_{\mathrm{s}}$ are given in Soulsby (1997). We have extended Soulsby and van Rijn expression for $u_{\mathrm{stir}}$ in Eq. (8) to include an extra contribution due to the stirring of sediment created by the roller-induced turbulence, which can produce significant sediment resuspension (Voulgaris and Collins 2000; Butt et al. 2004),

$$u_{\mathrm{stir}} = \sqrt{|\vec{v}|^2 + 0.018 c_D^{-1} u_b^2 + n_{\mathrm{rol}} u_{\mathrm{rol}}^2}\,. \tag{9}$$

Here, $u_{\mathrm{rol}}$ is a representative velocity of the turbulent bores created after the roller energy is dissipated and $n_{\mathrm{rol}}$ is a constant parameter. We follow (Roelvink and Stive 1989) and (Reniers et al. 2004), who assumed that this extra $u_{\mathrm{rol}}$ was proportional to the dissipation of roller energy, i.e.,

$$u_{\mathrm{rol}}^2 = \left(\frac{\mathcal{D}^{\mathrm{r}}}{\rho}\right)^{\frac{2}{3}}\left(e^{(D/H)} - 1\right)^{-1}\,, \tag{10}$$

where the exponential function accounts for the decrease of the turbulent velocity from the surface to the bed. By varying the parameter $n_{\mathrm{rol}}$ in Eq. (9), we can change the strength of the sediment resuspension due to roller-induced turbulence. Values of $n_{\mathrm{rol}}$ of about 40 give reasonable values of $\mathcal{C}$ in the inner surf zone of the order of $5\,10^{-3}$ m. The original Soulsby and van Rijn expression for $\mathcal{C}$ is obtained with $n_{\mathrm{rol}} = 0$. The Manning-Strickler law is again assumed for the drag coefficient $c_D$ in Eq. (9).

The coefficient $\Gamma$ in Eq. (7) has also been extended to include the effect of the surface rollers. Its default value yields bedslope coefficients similar in magnitude as those of the original Soulsby and van Rijn formulation (Soulsby 1997).

The Eqs. (1)–(6), together with the parameterizations used, define a closed dynamical system for the variables $z_{\mathrm{s}}$, $\mathbf{v}$, $\Phi$, $E$, $E_{\mathrm{r}}$ and $z_{\mathrm{b}}$. The fluid velocities are imposed to vanish at both the coastline and the offshore boundary, were we also assume a fixed bed level. Also, $z_{\mathrm{s}}$ and $E^{\mathrm{r}}$ are assumed to vanish at the offshore boundary, where wave conditions are prescribed ($H_{\mathrm{off}}$, $\theta_{\mathrm{off}}$, and $\omega_{\mathrm{a}} = 2\pi/T_{\mathrm{p}}$, where $T_{\mathrm{p}}$ is the peak wave period). The offshore boundary is at the location of the Gold Coast buoy (18-m depth).

### 4.3 Methodology

The model is applied to the Gold Coast conditions to be able to contrast its results with the data results of Section 3 and answer the research question. The default values and range of variation of the model parameters can be seen in Table 3. The default offshore wave conditions ($H_{\mathrm{off}} = 0.8$ m, $T_{\mathrm{p}} = 9$ s, and $\theta_{\mathrm{off}} = 30^o$) are the mean values measured at the Gold coast at the start of the finger bar events (Table 1). The default values of the physical parameters of the model parameterizations are the same that were used in

the previous applications of Duck and Noordwijk (Ribas et al. 2011a, 2012) and were a result of a model calibration with data from a Dutch beach close to Noordwijk (Ribas et al. 2011b).

The stability analysis approach to the formation of bars by self-organization starts by defining a steady and alongshore uniform basic state (i.e., without alongshore rhythmic bathymetry). In this study, the bed level profile, $z_b^o(x)$, shown in the lower panel of Fig. 8 was used, as it is a representative of the subtidal bathymetry measured at the Gold Coast in June 2002 (Fig. 3) at $y = -700$ m. Around that location, a finger bar event occurred 5 days before the bathymetric survey (Fig. 2). The shoreline of the modeled profile is assumed to be the terrace edge of the low-tide terrace. Recall that, at the Gold Coast, finger bars were attached to the low-tide terrace most of the time. The basic state solution is characterized by the presence of a longshore current, $\mathbf{v}^o = (0, V^o(x))$, and an elevation of the free surface level (i.e., the setup), $z_s^o(x)$. The superscript $^o$ denotes the basic state variables. This basic state only represents a morphodynamic equilibrium if it is assumed that the net cross-shore sediment flux vanishes.

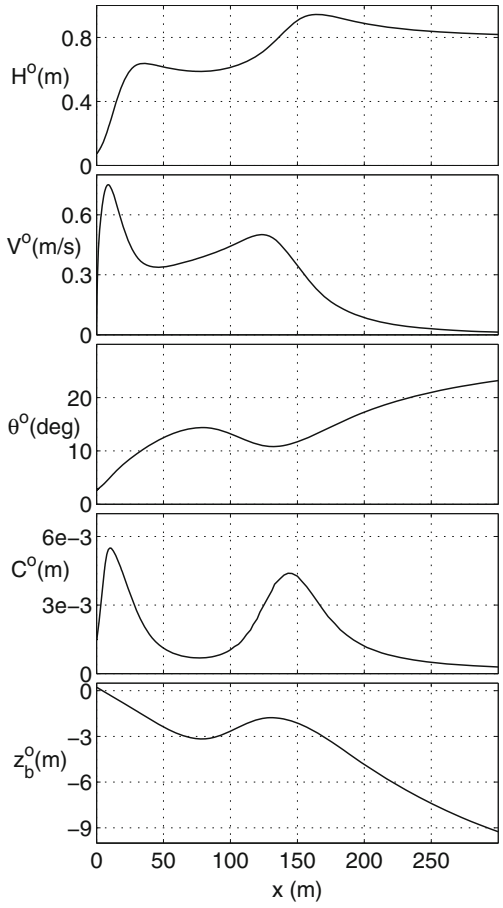


**Fig. 8** Cross-shore distribution of the basic state solution corresponding to the default parameter setting. Solution for (from *top to bottom*) the RMS wave height, $H^o$, the longshore current, $V^o$, the wave angle from the shore-normal, $\theta^\circ$, the depth-integrated sediment concentration, $C^o$, and the bed level, $z_b^o$

Once the basic state has been computed, the linear stability analysis is applied in a standard way. A small perturbation, assumed to be periodic in time and in the alongshore coordinate, is added to this state. For instance, for the bed level, this reads

$$z_\mathrm{b}(x, y, t) = z_\mathrm{b}^o(x) + \Re e(e^{\omega t + i\kappa y}\, h(x)) \,, \tag{11}$$

where $h$ stands for the cross-shore distribution of the perturbations of $z_\mathrm{b}$, $\kappa$ is the alongshore wavenumber of these perturbations, and $\omega$ is a complex growth rate. Expressions similar to Eq. (11) are used for the other six variables, where $\phi(x)$, $e(x)$, $e^r(x)$, $\eta(x)$, $u(x)$ and $v(x)$ correspond to the cross-shore structure of the perturbations in $\Phi$, $E$, $E^\mathrm{r}$, $z_\mathrm{s}$, $v_1$ and $v_2$, respectively. By inserting all the expressions like Eq. (11) in the governing equations, and linearizing with respect to the perturbations, an eigenproblem is obtained. For each $\kappa$, different complex eigenvalues $\omega$ exist, which characterize the different growing modes. The $e$-folding growth rate of the emerging bars is given by $\Omega = \Re e(\omega)$, so that $\Omega > 0$ implies growth. In case of an unstable basic state, solutions with $\Omega > 0$ are found and the growth rate curves show these positive $\Omega$ for different values of $\kappa$. Starting from arbitrary initial conditions, the dynamics after some time is assumed to be dominated by the mode with largest growth rate, $\Omega_M$, and the corresponding alongshore wavenumber $\kappa_M$. This fastest growing solution is the one that can be compared with the observed finger bars. Its $e$-folding growth time is given by $\tau_M = \Omega_M^{-1}$ and its migration speed by $c_M = -\Im m(\omega_M)/\kappa_M$. The alongshore wavelength of the corresponding bar patch is $\lambda_M = 2\pi/\kappa_M$, and the shape of the bar pattern and the associated quantities are given by Eq. (11). Given the uncertainties in the parameterizations used in the sediment transport formula, the function $\mathcal{C}$ in Eq. (7) is not perturbed.

## 5 Model results

### 5.1 Default case study

The basic state solution obtained for the default values of the parameters consists of a wave height profile, $H^o$, showing dissipation over the outer bar and at the terrace edge (Fig. 8). Correspondingly, peaks of the alongshore current, $V^o$, and the depth-integrated concentration, $C^o$, occur near these two locations. The extra sediment resuspension by rollers produces an increase in $C^o$ at the inner surf zone.

The linear stability analysis corresponding to the default parameter setting produces a dominant growing solution consisting of a patch of up-current finger bars with an

alongshore wavelength of $\lambda_{M1} = 85$ m (Fig. 9). The computed maximum growth rate is $\Omega_{M1} = 0.15$ h$^{-1}$, corresponding to an e-folding growth time of $\tau_{M1} = 6.6$ h. The modeled migration rate of this bar patch is $c_{M1} = 1.8$ m $h^{-1}$. The grayscale pattern in Fig. 9c shows the shape of the topographic perturbation corresponding to this fastest growing solution, and the small arrows display the perturbations of the current. As can be seen, seaward (shoreward) directed flow perturbations are obtained over the crests (troughs) of the finger bars. Note that the actual bed level is obtained by adding the bed level perturbation to the basic state bed level, $z_b^o$. The same applies to the flow: the longshore current $V^o$ must be added to the current perturbations to obtain the total flow. Note that linear stability analysis does not provide the finite amplitude of the perturbations.

A secondary maximum is obtained in the growth rate curve (Fig. 9a), which corresponds to the molding of the outer shore-parallel bar into a crescentic bar (its shape is shown in Fig. 9d). Its spacing is $\lambda_{M2} = 630$ m, in the range observed at the Gold Coast by Ruessink et al. (2007). The $e$-folding growth time is $\tau_{M2} = 10$ h and the migration rate is $c_{M2} = 19$ m h$^{-1}$. Note the difference in flow pattern between transverse and crescentic bars; in the latter case, offshore directed current perturbations occur over the troughs. The focus of this study are transverse finger bars, hence the crescentic bar solution will not be discussed in the rest of the paper.

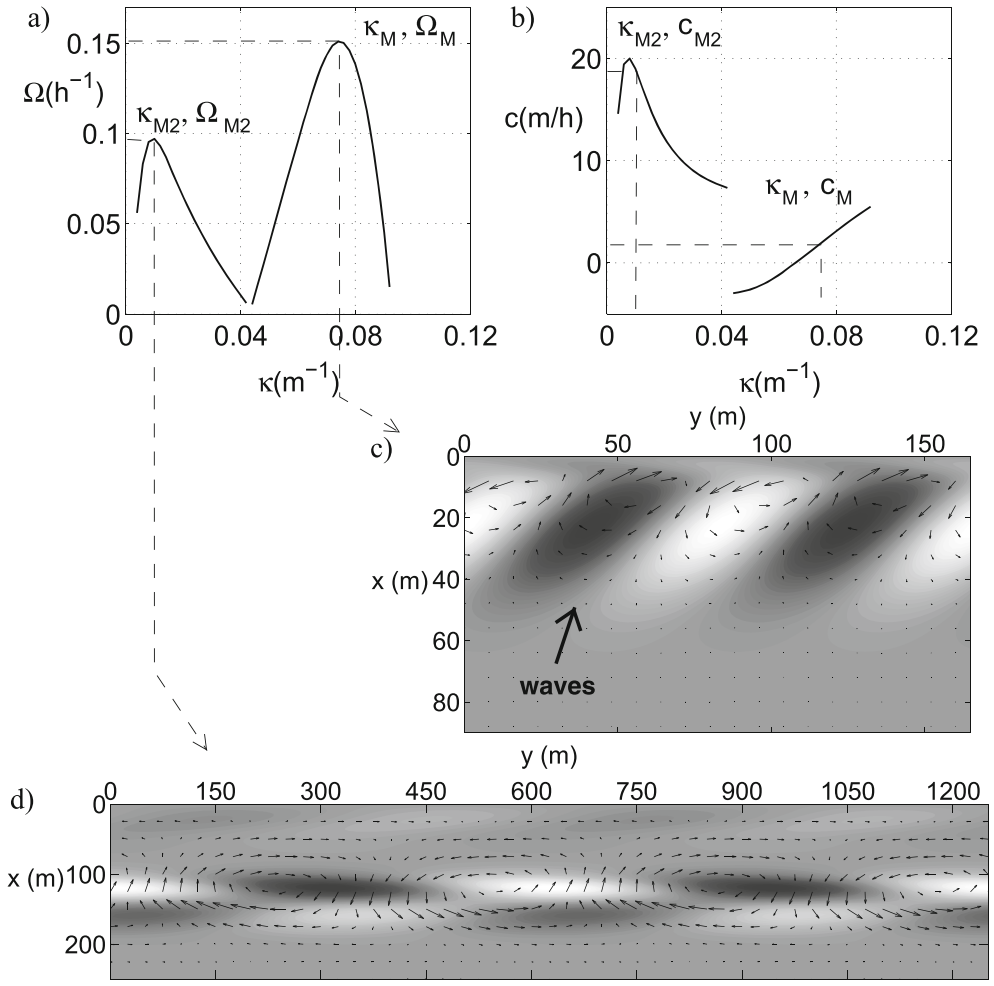


**Fig. 9** Results of the linear stability analysis for the default case. The growth rate curve (panel **a**, displaying $\Omega$ versus $\kappa$) and the migration rate curve (panel **b**, displaying $c$ versus $\kappa$) show the existence of two different modes. Panel **c** displays the topographic and current perturbations corresponding to the fastest growing mode, a patch of up-current oriented finger bars. Panel **d** shows the perturbations corresponding to the secondary mode, a crescentic bar. In the two latter plots, the shoreline $x = 0$ is at the top. Waves approach the coast from the lower left corner so the induced mean longshore current is directed from left to right. In the topographic perturbations, white areas indicate crests and dark areas represent troughs. Small arrows are the deviations of the longshore current induced by the growing bars

### 5.2 Influence of the physical parameters of the model

In order to simulate the variability in beach characteristics, the offshore wave conditions were varied within the range measured in the field (Tables 1 and 3). Each parameter ($H_{\text{off}}$, $T_{\text{p}}$, and $\theta_{\text{off}}$) was varied, keeping the other two equal to their default values. Given the known influence of the bed level profiles in finger bar formation (Ribas et al. 2012), all simulations were performed for three cross-shore bed level profiles: those corresponding to $y = -800$ m, $y = -700$ m (default one) and $y = -600$ m of the 2002 bathymetric survey (Fig. 3). These were the alongshore positions around the location of the finger bar event that was observed 5 days before the survey.

Transverse finger bars form when the offshore wave height is larger than about 0.5 m and the offshore wave angle is larger than 20° (Fig. 10). In general, higher growth and migration rates are found for higher $H_{\text{off}}$ and for increasing $\theta_{\text{off}}$ up to $40-60°$ ($\Omega_M$ and $c_M$ decreasing afterwards). Thereby, if the wave conditions are varied, the strength of the longshore current (which increases for larger $H_{\text{off}}$ and $\theta_{\text{off}}$ up to $40-60°$) determines the growth and migration rates, as occurred in Duck and Noordwijk (Ribas et al. 2011a, 2012). The modeled wavelength varies some 50 and 30 % when varying $H_{\text{off}}$ and $\theta_{\text{off}}$, respectively. The wave period has a smaller influence on finger bar characteristics. Changing the bed level profile also provides a variability of $\Omega_M$ (some 30 %) and $\lambda_M$ (some 50 %), of the same order as the variability produced by changes in the wave conditions (Fig. 10). The migration rate is less sensitive to varying the profile.

The value of the turbulence-induced stirring parameter, $n_{\text{rol}}$ in Eq. (9), was also varied, given the limited experimental knowledge of this phenomenon (Fig. 11). Finger

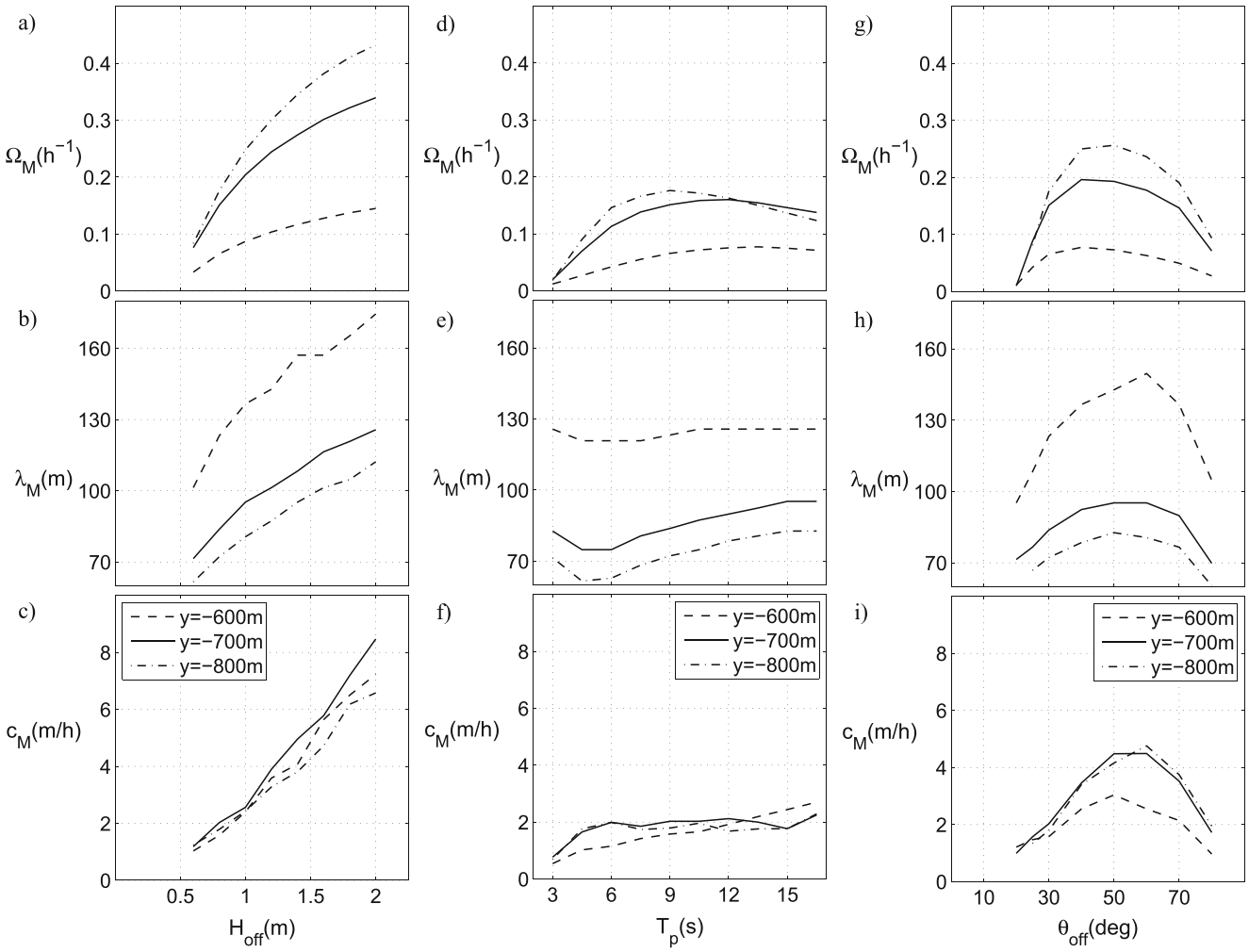


**Fig. 10** Sensitivity of the characteristics of modeled up-current oriented bars to varying the offshore wave height, $H_{\text{off}}$ (panels a–c), period, $T_{\text{p}}$ (panels d–f), and angle, $\theta_{\text{off}}$ (panels g–i). The *panels* show, from *top to bottom*, the sensitivity of $\Omega_M$ (panels a, d, and g), $\lambda_M$ (panels b, e, and h), and $c_M$ (panels c, f, and i). The *curves* correspond to different topographic profiles obtained at different alongshore positions of the 2002 bathymetry (Fig. 3), where the solid line ($y = -700$ m) is the default profile

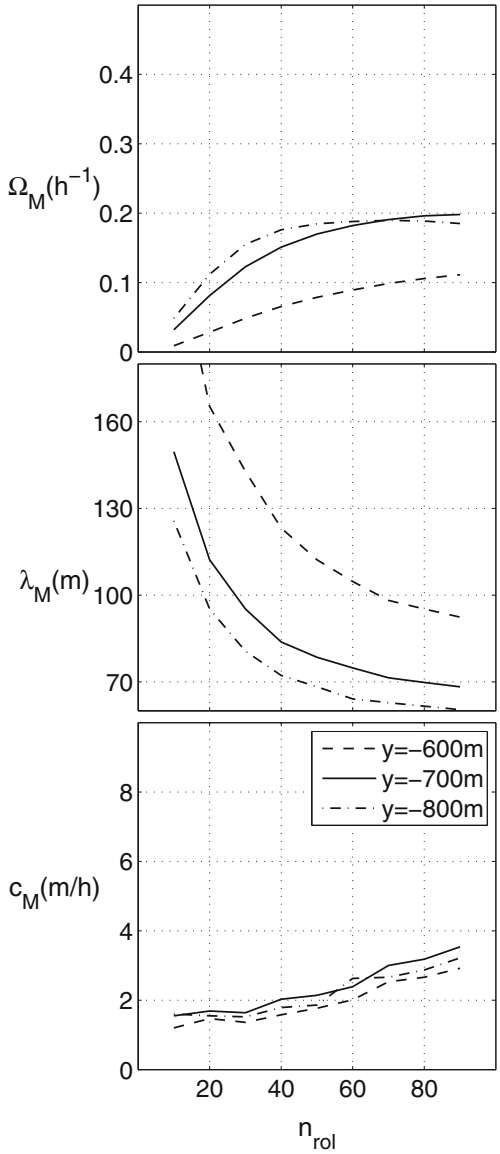


**Fig. 11** Sensitivity of the characteristics of modeled up-current oriented bars to varying the roller-induced turbulence stirring parameter ($n_{rol}$ in Eq. (9)). The *panels* show, from *top to bottom*, the sensitivity of $\Omega_M$, $\lambda_M$, and $c_M$. The *curves* correspond to different topographic profiles obtained at different alongshore positions of the 2002 bathymetry (Fig. 3), where the solid line ($y = -700$ m) is the default profile

bars are not formed if the value of this parameter is zero, which means that the formation of these bars cannot be modeled with the original Soulsby van Rijn sediment transport formula. In the case that $n_{rol} > 10$, the growth and migration rates of the bars become larger and their wavelengths decrease for increasing $n_{rol}$. Thereby, the sediment resuspension by roller-induced turbulence promotes the shoreward increase in depth-averaged sediment concentration necessary for transverse bars to form, as occurred in Duck and Noordwijk (Ribas et al. 2011a, 2012). The other model parameter related to the presence of surface rollers, the slope of the roller surface, $\beta_{rol}$, is also varied, and bar characteristics remain unchanged (not shown).

In order to check the robustness of bar characteristics, the sensitivity of model results to varying the value of three other model parameters (the apparent bed roughness, $k_a$, the turbulence parameter, $M$, and the saturation ratio, $\gamma_b$) was checked. The formation of transverse bars occurs for most of the range of realistic values of these parameters. Increasing $k_a$ and $M$ causes the longshore current magnitude to decrease and results in smaller growth and migration rates of the transverse bars. Increasing $\gamma_b$ allows for greater values of $H$ and hence of the longshore current, and this increases the values of $\Omega_M$ and $c_M$. The up-current oriented shape of the modeled bars is robust under changes of model parameters (provided that $n_{rol} > 10$).

## 6 Discussion

The observations of finger bars at the Gold Coast can be compared with the previous observations at Duck (Konicki and Holman 2000) and Noordwijk (Ribas and Kroon 2007) beaches. Transverse finger bars are observed substantially more often than in the earlier observations, with a larger percentage of days with finger bar events (24 % at Gold Coast, 14 % at Noordwijk, and 10 % and Duck) and a larger number of bars per patch (3–15 at the Gold Coast, 3–9 at Noordwijk, and 1–4 at Duck). Note that, in the analysis of finger bar data from Noordwijk and the Gold Coast, the criterion for bar detection was more restrictive than that in the analysis of Duck data. The wavelength is similar to that measured in Noordwijk but smaller than that measured in Duck (Table 4). Bars at the Gold Coast are up-current oriented, as occurred in Noordwijk (this was not measured at Duck). Migration rates have not been

**Table 4** Comparison of Gold Coast results with the earlier observations at Duck and Noordwijk

| Observation results | | | |
|---|---|---|---|
| Site | Wavelength (m) | Orientation | Migration rate[a] (m/h) |
| Gold Coast | 17–70 | up-current | – |
| Noordwijk | 21–75 | up-current | 0–1 |
| Duck | 12–180 | – | 0–1.7 |
| Model results | | | |
| Site | Wavelength (m) | Orientation | Migration rate (m/h) |
| Gold Coast | 60–170 | up-current | 1–8 |
| Noordwijk | 30–70 | up-current | 0.5–2 |
| Duck | 60–140 | up-current | 1–20 |

[a]Observed migration rates are daily averaged

measured at the Gold Coast but visual analysis of the events indicate very low migration of the bar patches, while bar patches migrated substantially in the other two sites. Wave conditions leading to finger bar presence in the Gold Coast observations are similar to what was observed in Noordwijk. There is some uncertainty in determining the wave conditions prior to bar formation because video images do not allow to observe the initial steps of bar formation (bars are visible in the images only when their amplitude is already significant). For this same reason, the characteristic growth time of finger bar formation cannot be measured in the video images. An estimation of the growth time is the typical duration of the required wave conditions leading to bar formation, which is of the order of 1 day. Data analysis in the Gold Coast has been performed in a simplified way compared with the analysis at Noordwijk and Duck. Further work on the Gold Coast finger bars should include a quantitative measurement of their orientation and migration together with a more quantitative relationship with climate indicators.

The differences in finger bar characteristics in the three sites might be due to the different bathymetric conditions, but it is difficult to contrast this hypothesis because, typically, the available bathymetric surveys are scarce. In fact, a novelty of the present data is that the large-scale beach configuration during finger bar presence was analyzed using a preexisting data set of beach states at Surfers Paradise, extracted from video-images by Price and Ruessink (2011). There is an indication that the presence of a strongly undulating outer bar coupled to a rhythmic low-tide terrace might favor finger bar formation (Fig. 7). However, this result must be taken with care because both this beach state and finger bars are typical features of low to intermediate wave conditions. A more robust result is that finger bars typically formed in the shoreward pointing embayments of the low-tide terrace instead of at its seaward directed perturbations. This is consistent with observations at Duck and Noordwijk, where formation of finger bars only occurred when the distance between the shoreline and the alongshore bar was larger than a critical value (Konicki and Holman 2000; Ribas and Kroon 2007). In any case, the Gold Coast often shows strongly rhythmic beach states (with the outer bar being most often in a transverse bar and rip state coupled to a rhythmic low-tide terrace), whereas the bars at Noordwijk and Duck are more often alongshore uniform or slightly undulating (e.g., compare Price and Ruessink (2011) with van Enckevort and Ruessink (2003)). Thereby, it might very well be that finger bar formation at the Gold Coast is influenced by the large-scale beach configuration and, in particular, this could explain why finger bars there do not migrate significantly.

In order to answer if the self-organization mechanism that explained finger bar formation at Duck (Ribas et al. 2011a) and Noordwijk (Ribas et al. 2012) is also applicable to the present data, the model that was applied to those two sites has been employed with the same parameter setting for the model parameterizations. The overall characteristics of finger bars observed at the Gold Coast, i.e., shape (up-current orientation), growth rate, and wave conditions leading to their formation, are relatively well reproduced by the model. Consequently, similar as in Duck and Noordwijk, formation of finger bars can be explained (at least partially) by the following physical mechanism. The longshore current, induced by obliquely incident breaking waves, deflects offshore over the crest of the finger bars (Fig. 9c). This flow deflection, together with a depth-averaged sediment concentration that decreases in the seaward direction (promoted by roller-induced sediment resuspension), explains the growth of finger bars with an up-current orientation. A more detailed description of the physical mechanism can be found in Ribas et al. (2012).

Modeled bar characteristics at the three sites are also compared in Table 4. The present results are more similar to the model results obtained at Duck beach. Instead, the model results at Noordwijk showed smaller modeled wavelengths and migration rates, which both were closer to the range of observed values. Two important differences between these beaches are that the Noordwijk bathymetry has a smaller inner surf zone slope (the default profiles had slopes of 0.02 in Noordwijk, 0.03 in Duck, and 0.04 at the Gold Coast) and a shallower bar (bar crest was located at 1.2-m depth in Noordwijk, at 2.5-m depth in Duck, and at 2-m depth at the Gold Coast). Another difference is that the Noordwijk default profile used in the model had two longshore bars, while those of the other two sites had only one. The sensitivity of the characteristics of modeled finger bars to varying the parameters is similar in the three beaches.

As occurred in the two earlier model applications, modelled growth rates increase with increasing offshore wave heights (Fig. 10), while finger bars in the field are not observed for $H_{\mathrm{off}} > 1.2$ m. These findings are not contradictory because an essential condition for finger bar formation is that both the wave incidence angle and the wave height are larger than a certain threshold. Such conditions only occur part of the time in the field. For instance, at Duck, it was shown that conditions for finger bar formation only occurred 25 % of the time (Ribas et al. 2011a). They also showed that large waves were most of the time shore-normal and that the small angle of wave incidence was what limited finger bar formation. A similar behavior occurred at Noordwijk: the wave conditions that were leading to finger bar formation in the field could be reproduced by taking into account not only the modeled wave conditions for growth but also the frequency of occurrence of each $H$-$\theta$ pair in the field (Ribas et al. 2012).

The model results at the Gold Coast do not reproduce accurately the observed wavelength (while wavelength was relatively well reproduced in the other two sites, Table 4) and modeled migration rates are large, while observed finger bars do not seem to migrate significantly. The reason why there are more discrepancies between model results and data at the Gold Coast might be because finger bars in this site are influenced by the large-scale beach configuration. This coupling cannot be reproduced with Morfo62 model because it is based on linear stability analysis, which assumes by definition an initially alongshore uniform bathymetry. There is also an important uncertainty associated to the shape of the bed level profiles. Only one bathymetric survey was available (close in time to a finger bar event) and the bed level can rapidly change at small water depths. At the same time, modeled bar characteristics are sensitive to the shape of the profile (Fig. 10). Finally, neglecting tidal variability also poses restrictions since finger bars evolve at similar time scales as tidal waves, and tides produce significant changes in water depth at the inner surf zone (this limitation also holds in the previous model applications to Duck and Noordwijk sites).

Future modeling studies of finger bars should use a nonlinear model (i.e., Garnier et al. 2006) and start with a more realistic initial bathymetry, incorporating preexisting larger-scale variability. With this tool, it could be investigated how the formation of transverse finger bars is affected by the large-scale beach configuration. Such nonlinear model could also incorporate more easily the effect of tides.

## 7 Conclusions

The formation of transverse finger bars in the surf zone of Surfers Paradise beach (Gold Coast, East Australia) has been investigated with Argus video observations and an existing morphodynamic model based on linear stability analysis (called Morfo62).

The video data comprise 4-year (November 1999-October 2003) set of daily, low-tide time-exposure video images and associated hourly records of offshore (in 18-m depth) wave height, period, and direction. Finger bars are observed during 24 % of the study period, substantially more often than in the earlier observations from Duck (USA) and Noordwijk (the Netherlands). They form in patches of up to 15 bars attached to the low-tide terrace, with an average lifetime of 5 days. The alongshore wavelength varies from 17 to 70 m, with a data set average value of 32 m (similar to finger bars at Noordwijk and half the wavelength at Duck). The offshore RMS wave height prior to the formation of finger bars never exceeds 1.2 m, indicating finger bars to be low to intermediate wave-energy features, as was observed at Duck and Noordwijk. The dominant angle of wave incidence prior to formation of finger bars varies between 12° and 44° from shore-normal. Finger bars are typically up-current oriented, i.e., their crests point toward the direction of the incident waves. In contrast with observations at Duck and Noordwijk, patches of finger bars at the Gold Coast do not migrate significantly. When finger bars are present, the low-tide terrace often (43 % of the time) displays alongshore variability of a few hundreds of meters, enforced by the variability in the onshore propagating outer bar.

In order to investigate if the self-organization mechanism that successfully explained finger bar formation at Duck and Noordwijk can also explain the growth of the Gold Coast bars, the morphodynamic model that was applied to the two earlier studies is also employed here. Using a bed level profile representative of the Gold Coast and the offshore RMS wave height, period, and angle of incidence measured at the start of finger bar events (0.8 m, 9 s, and 30°, respectively), the model produces up-current finger bars attached to the low-tide terrace with an alongshore wavelength of 85 m in the default case (2.5 times larger than the observed value). The default modeled e-folding growth time is 6 h, and the migration rate is 1.8 m $h^{-1}$. Simulations in which the offshore wave conditions are varied reveal that finger bars form if the offshore wave height is larger than 0.5 m and the offshore wave angle varies between 20° and 80°. Modeled growth rates increase when increasing the height and the angle of incidence of waves because the strength of the longshore current controls the growth rate of finger bars. The bed level profile is also changed, and it induces a variability in finger bar characteristics of the same order than the variability produced by varying the wave conditions. According to the model results, sediment resuspension by roller-induced turbulence promotes the increase in depth-averaged sediment concentration near the shoreline that is necessary for finger bars to form. This makes the depth-averaged sediment concentration to decrease in the seaward direction, enhancing the convergence of sediment transport in the offshore directed flow perturbations that occur over the up-current oriented bar crests. The overall characteristics of finger bars observed at the Gold Coast, i.e., shape (up-current orientation), growth rate, and wave conditions leading to their formation, are relatively well reproduced by the model. It is thus concluded that the self-organization mechanism behind finger bar formation at Duck and Noordwijk is also playing an important role in the formation of finger bars at the Gold Coast. However, the modeled values of the wavelength and the migration rate of the bars are larger than the observed values. The fact that finger bars at the Gold Coast are observed to coincide with clearly rhythmic bar states can explain these divergences. Finger bars in the field might be influenced by the large-scale beach

configuration and this is not taken into account in the linear model since it requires an alongshore uniform initial bathymetry.

**Acknowledgments** Funding from the Spanish research project 'Modelización y monitorización integradas en morfodinámica de playas naturales y regeneradas' (contract CTM2009-11892) and from the Netherlands Organization for Scientific Research NWO (contract 818.01.009) is acknowledged.

## References

Butt T, Russel P, Puleo J, Miles J, Masselink V (2004) The influence of bore turbulence on sediment transport in the swash and inner surf zones. Cont Shelf Res 24:757–771

Feddersen F, Guza RT, Elgar S, Herbers THC (2000) Velocity moments in alongshore bottom stress parameterizations. J Geophys Res 105(C4):8673–8686

Garnier R, Calvete D, Falqués A, Caballeria M (2006) Generation and nonlinear evolution of shore-oblique/transverse sand bars. J Fluid Mech 567:327–360

Konicki KM, Holman RA (2000) The statistics and kinematics of transverse bars on an open coast. Mar Geol 169:69–101

Price TD, Ruessink BG (2011) State dynamics of a double sandbar system. Cont Shelf Res 31:659–674

Reniers AJHM, Roelvink JA, Thornton EB (2004) Morphodynamic modeling of an embayed beach under wave group forcing. J Geophys Res 109(C01030). doi:10.1029/2002JC001586

Ribas F, Kroon A (2007) Characteristics and dynamics of surfzone transverse finger bars. J Geophys Res 112(F03028). doi:10.1029/2006JF000685

Ribas F, de Swart HE, Calvete D, Falqués A (2011a) Modelling the formation of transverse sand bars: application to Duck beach, USA. In Proc 7th IAHR Symp River, Coast Estuar Morphodynamics. Tsinghua University Press. In press

Ribas F, de Swart HE, Calvete D, Falqués A (2011b) Modelling waves, currents and sandbars on natural beaches: the effect of surface rollers. J Marine Syst 88:90–101. doi:10.1016/j.jmarsys.2011.02.016

Ribas F, de Swart HE, Calvete D, Falqués A (2012) Modeling and analyzing observed transverse sand bars in the surf zone. J Geophys Res 117(F02013). doi:10.1029/2011JF002158

Roelvink JA, Stive MJF (1989) Bar-generating cross-shore flow mechanisms on a beach. J Geophys Res 94(C4):4785–4800

Ruessink BG, Pape L, Turner IL (2009) Daily to interannual cross-shore sandbar migration: observations from a multiple sandbar system. Cont Shelf Res 29:1663–1677

Ruessink BG, Miles JR, Feddersen F, Guza RT, Elgar S (2001) Modeling the alongshore current on barred beaches. J Geophys Res 106(C10):22451–22463

Ruessink BG, Coco G, Ranasinghe R, Turner IL (2007) Coupled and noncoupled behavior of three-dimensional morphological patterns in a double sandbar system. J. Geophys. Res. 112(C07002). doi:10.1029/2006JC003799

Soulsby RL (1997) Dynamics of Marine Sands. Thomas Telford, London

Splinter KD, Holman RA, Plant NG (2011) A behavior oriented dynamic model for sandbar migration and 2DH evolution. J Geophys Res 116(C01020). doi:10.1029/2010JC006382

Svendsen IA (1984) Mass flux and undertow in the surf zone. Coast Eng 8:347–365

Thornton B, Guza RT (1983) Transformation of wave height distribution. J Geophys Res 88(10):5925–5938

van Enckevort IMJ, Ruessink BG (2003) Video observations of nearshore bar behaviour. Part 2: alongshore non-uniform variability. Cont Shelf Res 23:513–532

van Enckevort IMJ, Ruessink BG, Coco G, Suzuki K, Turner IL, Plant NG, Holman RA (2004) Observations of nearshore crescentic sandbars. J Geophys Res 109(C06028). doi:10.1029/2003JC002214

Voulgaris G, Collins MB (2000) Sediment resuspension on beaches: response to breaking waves. Mar Geol 167:167–187

Wright LD, Short AD (1984) Morphodynamic variability of surf zones and beaches: a synthesis. Mar Geol 56:93–118